Generalised curvilinear coordinates, vertical discretisations, and moving mesh adaptivity in atmospheric numerical models

Christian Kühnlein

ECMWF

Main topics of this lecture:

1. Governing PDEs of atmospheric dynamics in generalised curvilinear coordinates
2. Vertical coordinates/discretisation in atmospheric models
3. Adaptive (moving) meshes

Generalised curvilinear coordinate mappings

- ...transform governing PDEs to more convenient coordinates for solution
- ...accommodate complex boundaries
- ...apply a variable-resolution mesh
- ...apply dynamic mesh adaptivity

$$(\overline{x}, \overline{y}) = (E(x, y), D(x, y)) : \quad \mathcal{D}_p \to \mathcal{D}_t$$

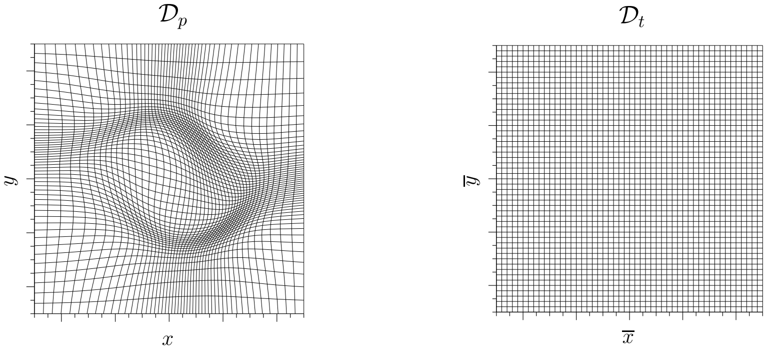

General bijective coordinate mapping:

$$(\bar{t}, \bar{\mathbf{x}}) = (t, \mathcal{F}(t, \mathbf{x})) : \quad \mathcal{D}_p \rightarrow \mathcal{D}_t$$

- $\mathcal{D}_p$ is subdomain of the physical space $\mathbf{S}_p$ – with coordinates $(t, \mathbf{x}) \equiv (t, x, y, z)$ and metric tensor g_{kj} – where the physical problem is posed. It is convenient to assume the physical system $\mathbf{S}_p$ to be a stationary and orthogonal (e.g. Cartesian, geospherical, spheroidal,..)

- $\mathcal{D}_t$ is subdomain of transformed computational space $\mathbf{S}_t$ – with generalised coordinates $(\bar{t}, \bar{\mathbf{x}}) \equiv (\bar{t}, \bar{x}, \bar{y}, \bar{z})$ and metric tensor $\overline{g}_{rs}$ – where the problem is solved

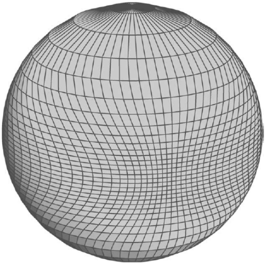

Symbolic vector-form of basic adiabatic governing PDEs:

$$\frac{D\mathbf{v}}{Dt} = -c_p\theta\nabla\pi + \mathbf{g} + \mathbf{M}$$

$$\frac{D\theta}{Dt} = 0$$

$$\frac{D\rho}{Dt} = -\rho\nabla\cdot\mathbf{v}$$

with

$$\mathbf{v} = (v^1, v^2, v^3)\ , \qquad \mathbf{g} = (0, 0, -g)$$

Transformed governing PDEs in $\mathbf{S}_t$ (e.g. Clark JCP 1977, Prusa et al. JCP 2003):

$$\frac{dv^j}{d\bar{t}} = -c_p\theta\tilde{G}_j^k\frac{\partial\pi}{\partial\bar{x}^k} - g\delta_3^j + M^j \qquad j = 1,2,3$$

$$\frac{d\theta}{d\bar{t}} = 0$$

$$\frac{d\rho}{d\bar{t}} = -\frac{\rho}{\overline{G}}\left(\frac{\partial\overline{G}\,\overline{v}^{s\,k}}{\partial\bar{x}^k}\right)$$

with

$$\frac{d}{d\bar{t}} = \frac{\partial}{\partial\bar{t}} + \overline{v}^{*\,k}\frac{\partial}{\partial\bar{x}^k}\;, \qquad \tilde{G}_j^k := \sqrt{g^{jj}}\frac{\partial\bar{x}^k}{\partial x^j} \qquad \overline{G} = |\overline{g}_{jk}|^{1/2}$$

$$\overline{v}^{*\,j} = \frac{d\bar{x}^j}{d\bar{t}} = \overline{v}^{s\,j} + \frac{\partial\bar{x}^j}{\partial t} \qquad \overline{v}^{s\,j} = \frac{\partial\bar{x}^j}{\partial x^k}v^{*\,k} \qquad v^k = \sqrt{g_{kk}}\,v^{*\,k}$$

$\rightarrow$ see e.g. textbook by Zdunkowski and Bott 2003 for fundamentals

Governing equations in Eulerian conservation form

Transformed governing PDEs in $\mathbf{S}_t$:

$$\frac{\partial \rho^* v^j}{\partial \overline{t}} + \overline{\nabla} \cdot \left(\overline{\mathbf{v}}^* \rho^* v^j \right) = -\rho^* c_p \theta \tilde{G}_j^k \frac{\partial \pi}{\partial \overline{x}^k} - \rho^* g \delta_3^j + \rho^* M^j \qquad j = 1, 2, 3$$

$$\frac{\partial \rho^* \theta}{\partial \overline{t}} + \overline{\nabla} \cdot (\overline{\mathbf{v}}^* \rho^* \theta) = 0$$

$$\frac{\partial \rho^*}{\partial \overline{t}} + \overline{\nabla} \cdot (\overline{\mathbf{v}}^* \rho^*) = 0$$

with

$$\overline{\nabla} \equiv \left(\frac{\partial}{\partial \overline{x}}, \frac{\partial}{\partial \overline{y}}, \frac{\partial}{\partial \overline{z}} \right) \,, \qquad \overline{\mathbf{v}}^* \equiv \left(\overline{v}^{*1}, \overline{v}^{*2}, \overline{v}^{*3} \right) \,, \qquad \rho^* \equiv \overline{G} \rho$$

Tensor identities

1. Divergence in generalised coordinates:

$$\nabla \cdot \mathbf{A} = \frac{1}{\overline{G}} \frac{\partial}{\partial \overline{x}^k} \left(\overline{G}\, \overline{A}^k \right) - \overline{A}^j \left[\frac{G}{\overline{G}} \frac{\partial}{\partial \overline{x}^k} \left(\frac{\overline{G}}{G} \frac{\partial \overline{x}^k}{\partial x^j} \right) \right]$$

Invariance of divergence uses multi-component geometric conservation law (GCL):

$$\frac{G}{\overline{G}} \frac{\partial}{\partial \overline{x}^k} \left(\frac{\overline{G}}{G} \frac{\partial \overline{x}^k}{\partial x^j} \right) \equiv 0$$

2. Reciprocity of covariant and contravariant base vectors:

$$\overline{\mathbf{q}}^r \cdot \overline{\mathbf{q}}_s = \frac{\partial \overline{x}^r}{\partial x^q} \frac{\partial x^q}{\partial \overline{x}^s} = \delta^r_s$$

$\rightarrow$ Discrete model should respect these identities ! (see e.g. Thomas and Lombard 1979, Prusa and Gutowski IJNMF 2006, Kühnlein et al. JCP 2012)

Vertical coordinates in atmospheric models

→ Independent vertical variable ζ

$$(\overline{x}, \overline{y}, \zeta) = (x, y, \zeta(t, x, y, z))$$

- height z
- (hydrostatic) pressure p
- potential temperature θ
- ...

→ Terrain-following coordinates

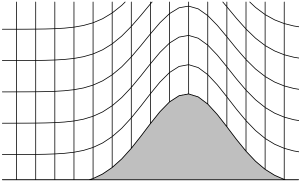

+ levels do not intersect the earth's surface
+ specification of the lower boundary condition
+ uniform vertical mesh spacing near the surface
+ stretching easily allows higher resolution towards the surface
+ long time steps

(-) potential errors in pressure gradient term
(-) mesh quality for steep orography

Gal-Chen and Somerville terrain-following vertical coordinate

Terrain-following coordinate of Gal-Chen and Somerville (1975):

$$\overline{z} = \overline{z}(x, y, z) = H \frac{z - h(x, y)}{H - h(x, y)}$$

with inverse mapping

$$z = z(x, y, \overline{z}) = \overline{z} + \left(1 - \frac{\overline{z}}{H}\right) h = \overline{z} + b(\overline{z}) h(x, y)$$

H: height of model top
$h(x, y)$: local height of orography
$b(\overline{z})$: vertical decay function of orography

Gal-Chen and Somerville terrain-following vertical coordinate

West-east cross section through the Alps ($\Delta_h \sim 1.2$ km)

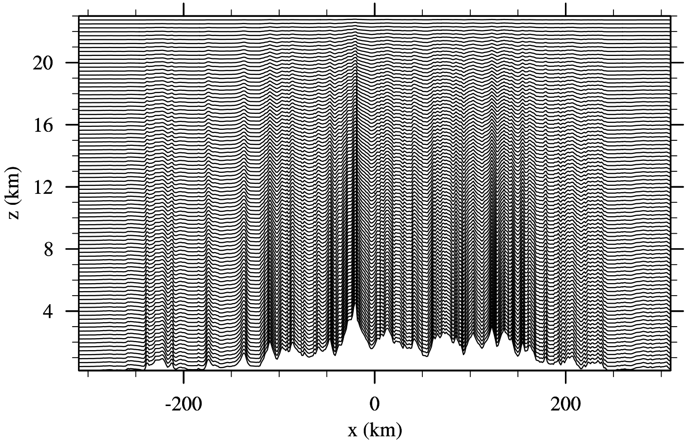

Gal-Chen and Somerville terrain-following vertical coordinate

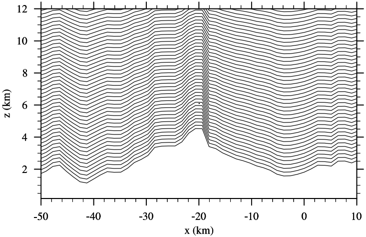

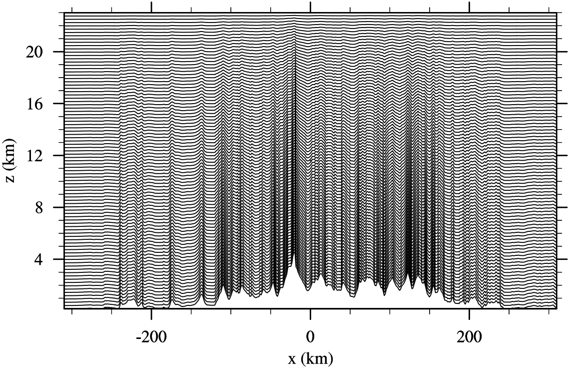

Gal-Chen and Somerville terrain-following vertical coordinate

Hybrid specification:

$$z(x, y, \overline{z}) = \overline{z} + b(\overline{z})h(x, y)$$

where

$$b(\overline{z}) = \begin{cases} (1 - \overline{z}/H_r) & : \overline{z} \leq H_r \\ 0 & : \overline{z} > H_r \end{cases}$$

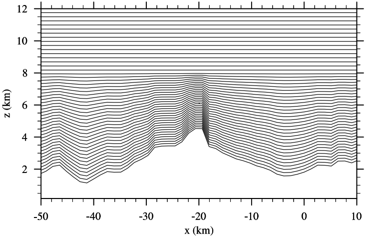

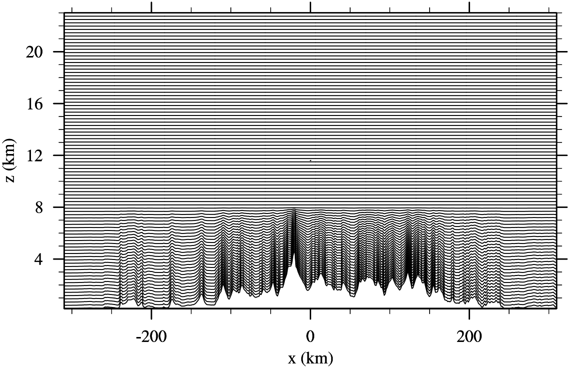

Smoothed height-based terrain-following coordinates

Smoothed coordinate – SLEVE (Schär et al. MWR 2002, Leuenberger et al. MWR 2010):

$$z(x, y, \overline{z}) = \overline{z} + b_s h_s(x, y) + b_r h_r(x, y)$$

h_s : smoothed terrain

$h_r = h - h_s$: residual containing small-scale variations of terrain

b_s : vertical decay function for h_s

b_r : vertical decay function for h_r

with

$$b_i(\overline{z}) = \frac{\sinh\left[(H/s_i)^n - (\overline{z}/s_i)^n\right]}{\sinh\left[(H/s_i)^n\right]}$$

$\Rightarrow$ Faster decay for b_r versus b_s by defining smaller scale-height s_i

See also: Zängl MWR 2003, Klemp MWR 2011

SLEVE coordinate

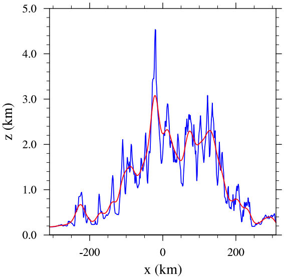

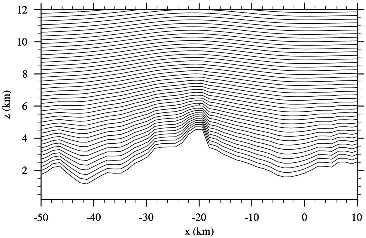

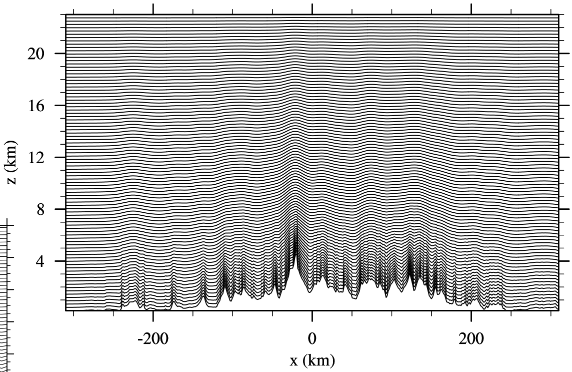

SLEVE in hybrid setting with vertical stretching:

$$\tilde{z} = C^{-1}(\bar{z}) \quad \rightarrow \quad z = z(x, y, \tilde{z})$$

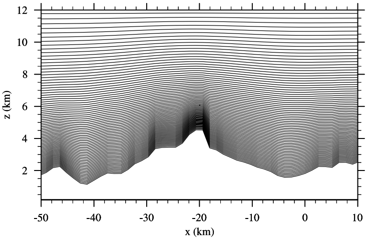

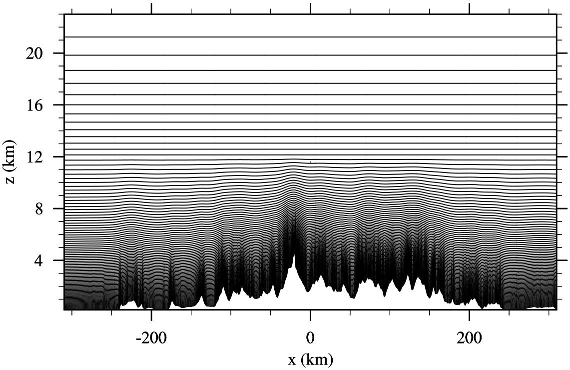

Pressure-based terrain-following vertical coordinate η of the form:

$$(\overline{x}, \overline{y}, \eta) \equiv (x, y, \eta(p, p_s))$$

with $\qquad \eta_s = \eta(p_s, p_s) \equiv 1 \qquad \eta_t = \eta(p_t, p_s) \equiv 0$

$p(t, x, y, z)$: pressure, $p_s(t, x, y)$: surface pressure, p_t: top pressure
$\rightarrow$ bijective mapping between p and η for a given p_s.

One example is (Phillips JM 1957 "A coordinate system having some special advantages for numerical forecasting", Mintz 1965)

$$\sigma = \eta = \frac{p - p_t}{p_s - p_t}$$

commonly named as the σ-coordinate.

Hybrid σ-p vertical coordinate (Simmons and Burridge MWR 1981) employed in ECMWF's operational IFS model (with $p_t \equiv 0$):

$$p(t, x, y, z) = A(\eta) + B(\eta) p_s(t, x, y)$$

with

$$A(\eta_t) = 0 \ , \quad B(\eta_t) = 0 \ , \quad A(\eta_s) = 0 \ , \quad B(\eta_s) = 1$$

$\rightarrow$ terrain-following σ-like levels near the earth's surface with transition to pressure levels in the upper troposphere and stratosphere

- different approaches to specify A and B coefficients (see e.g. Eckermann MWR 2009)
- similar in non-hydrostatic models (Laprise MWR 1992, Bubnova et al. MWR 1995)

Hybrid pressure-based terrain-following coordinates

Evolution of hybrid $\sigma - p$ levels of IFS over a 10 day T255/L91 forecast
(*Zonal section at* $\sim$*60° N*)

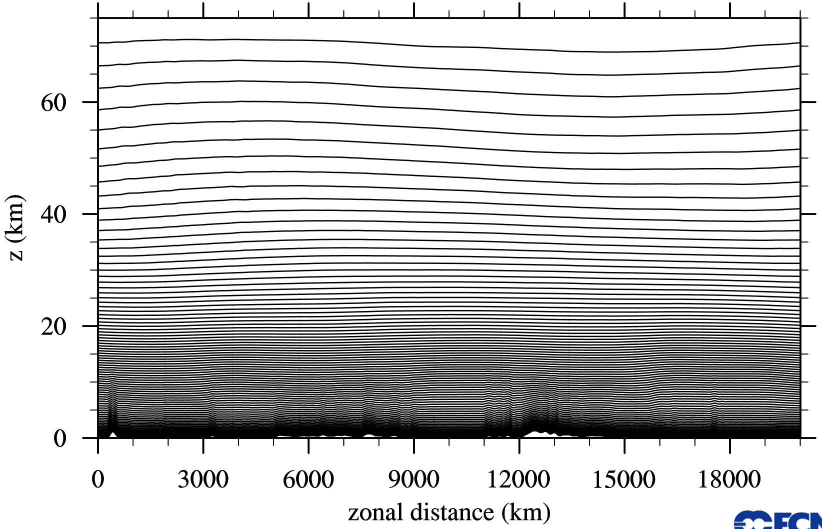

Isentropic vertical coordinates

Potential temperature θ as independent vertical coordinate:

- for inviscid adiabatic flow $D\theta/Dt = 0$ isentropes represent material surfaces
- more accurate representation of vertical transport
- adaptive vertical mesh spacing proportional to thermal stratification
- implemented as hybrid terrain-following-θ coordinate
- becomes more complicated for high resolution due to small-scale θ variations
- regularisation of coordinate required to ensure monotonicity

$\rightarrow$ see e.g. Hsu and Arakawa, MWR 1990; Konor and Arakawa, MWR 1997; Benjamin et al. MWR 2004; Toy and Randall MWR 2009

ECMWF

Pressure gradient term with terrain-following coordinates

⇒ horizontal pressure gradient

$$-c_p\theta\frac{\partial\pi}{\partial x} = -c_p\theta\left(\frac{\partial\pi}{\partial\overline{x}} + \frac{\partial\overline{z}}{\partial x}\frac{\partial\pi}{\partial\overline{z}}\right)$$

susceptible to errors

+ subtraction of balanced state
+ satisfy tensor identities, consistency of discrete metrics and dynamics (see e.g. Prusa and Gutowski IJNMF 2006; Klemp et al. MWR 2003)
+ boundary conditions (e.g. Smolarkiewicz et al. JCP 2007)
+ smoothed coordinate levels
+ truly horizontal evaluation of horizontal components of the pressure gradient and horizontal diffusion using reconstructed quantities on Cartesian mesh (Zängl MWR 2012, and references therein)
+ see also Weller and Shahrokhi MWR 2014

Steep orography with a basic terrain-following vertical coordinate

Stratified flow past isolated mountain on a small planet (max. slope ∼37°)

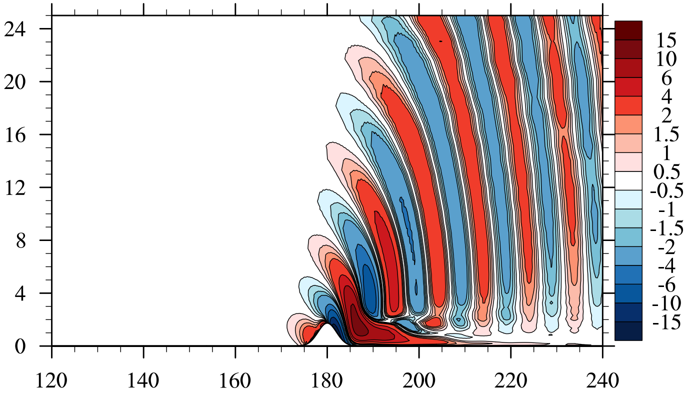

→ Basic terrain-following coordinate, semi-implicit integration of Euler equations (Smolarkiewicz et al. 2014), finite-volume MPDATA scheme (Kühnlein and Smolarkiewicz 2017), no explicit diffusion

Steep orography with a basic terrain-following vertical coordinate

Stratified flow past isolated mountain on a small planet (max. slope ∼71°)

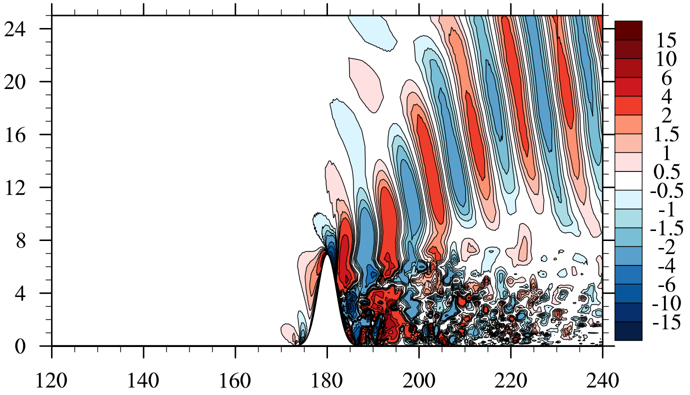

→ Basic terrain-following coordinate, semi-implicit integration of Euler equations (Smolarkiewicz et al. 2014), finite-volume MPDATA scheme (Kühnlein and Smolarkiewicz 2017), no explicit diffusion

→ Cut-cell method (e.g. Steppeler et al. 2002, Klein et al. 2009, Lock et al. 2012)

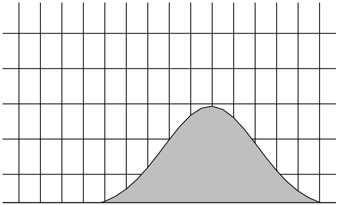

→ Slanted cell approach (Shaw and Weller MWR 2016, Shaw et al. 2017)

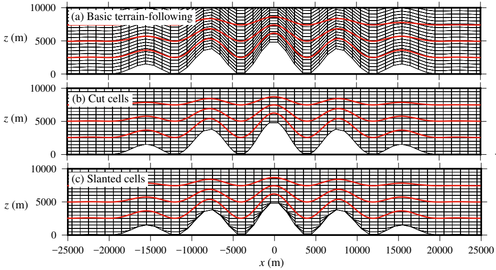

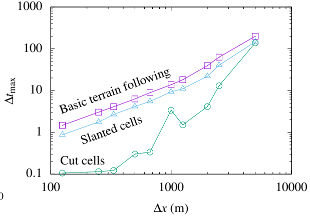

$\rightarrow$ 3D unstructured mesh discretisation $\rightarrow$ see J. Szmelter's lecture

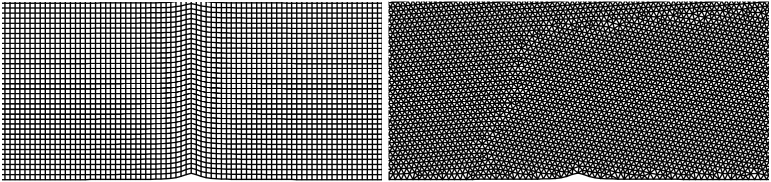

Multiscale atmospheric flows

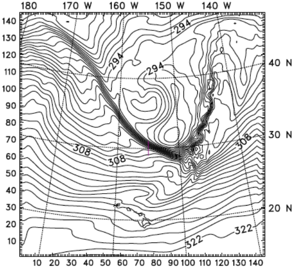

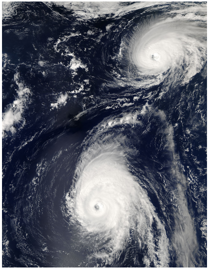

- → Extremely different local scales in atmospheric flows
- → Standard approach in atmospheric solvers of uniform mesh not optimal
- → Variable mesh applying locally finer/coarser spacing more efficient
- → Solution-adaptive mesh is able to conform to flow evolution

$$(\overline{x}, \overline{y}) = (E(t, x, y), D(t, x, y)) : \quad \mathcal{D}_p \to \mathcal{D}_t$$

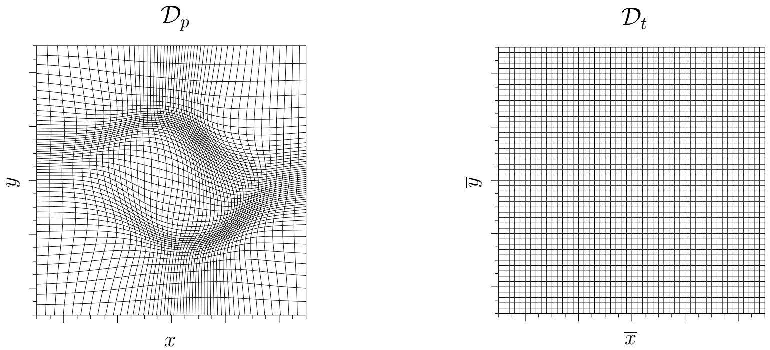

→ moving mesh or r-adaptive technique (see Budd et al. AN 2009 for comprehensive discussion)

Time-dependent deformational shear flow (Blossey and Durran, JCP 2008) using advection scheme MPDATA (Smolarkiewicz IJNMF 2006) with moving meshes (Kühnlein et al. JCP 2012):

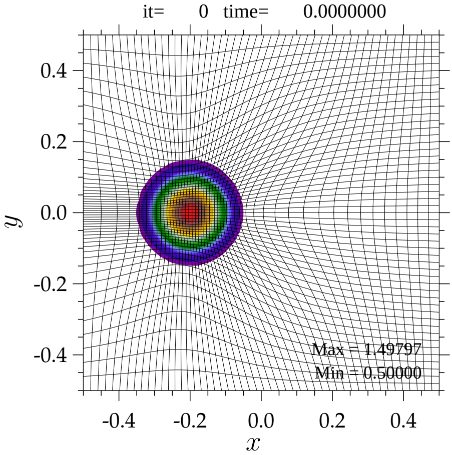

→ mesh refinement indicator: $\Phi = ||\nabla\psi||$

Scalar advection experiment

uniform mesh - 50^2, $T_{rw} = 1$

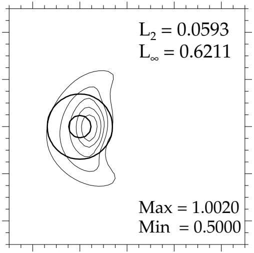

uniform mesh - 250^2, $T_{rw} = 133$

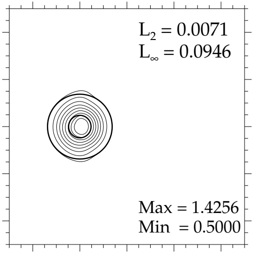

adaptive mesh - 50^2, $T_{rw} = 5.5$

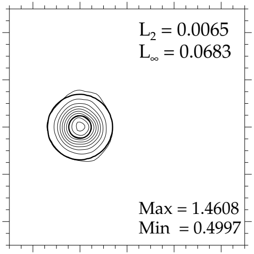

$\rightarrow$ T_{rw} is relative wall clock time to uniform mesh run with 50^2 mesh cells (leftmost panel)

Moving mesh PDEs

MMPDEs (Huang JCP 2001) govern time-dependent mapping (here 2D) from computational to physical space:

$$P(\mathbf{x}_h, M)\,\frac{\partial \mathbf{x}_h}{\partial \bar{t}} = \sum_{i,j=1,2} D_{ij}(\mathbf{x}_h, M)\,\frac{\partial^2 \mathbf{x}_h}{\partial \overline{x}^i \partial \overline{x}^j} + \sum_{i=1,2} C_i(\mathbf{x}_h, M)\,\frac{\partial \mathbf{x}_h}{\partial \overline{x}^i}$$

with coefficients

$$D_{ij}(\mathbf{x}_h, M) = \nabla_h \overline{x}^i \cdot M^{-1}\,\nabla_h \overline{x}^j\ , \qquad C_i(\mathbf{x}_h, M) = -\nabla_h \overline{x}^i \cdot \left(\sum_{k=1,2} \frac{\partial M^{-1}}{\partial \overline{x}^k}\,\nabla_h \overline{x}^k \right)\ ,$$

$$P(\mathbf{x}_h, M) = \mathcal{T}\,\sqrt{(D_{11})^2 + (D_{22})^2 + (C_1)^2 + (C_2)^2}$$

Moving mesh PDEs

MMPDEs (Huang JCP 2001) govern time-dependent mapping (here 2D) from computational to physical space:

$$P(\mathbf{x}_h, M)\,\frac{\partial \mathbf{x}_h}{\partial \bar{t}} = \sum_{i,j=1,2} D_{ij}(\mathbf{x}_h, M)\,\frac{\partial^2 \mathbf{x}_h}{\partial \bar{x}^i \partial \bar{x}^j} + \sum_{i=1,2} C_i(\mathbf{x}_h, M)\,\frac{\partial \mathbf{x}_h}{\partial \bar{x}^i}$$

with coefficients

$$D_{ij}(\mathbf{x}_h, M) = \nabla_h\,\bar{x}^i \cdot M^{-1}\,\nabla_h\,\bar{x}^j\ , \qquad C_i(\mathbf{x}_h, M) = -\nabla_h\,\bar{x}^i \cdot \left(\sum_{k=1,2} \frac{\partial M^{-1}}{\partial \bar{x}^k}\,\nabla_h\,\bar{x}^k\right)\ ,$$

$$P(\mathbf{x}_h, M) = \mathcal{T}\,\sqrt{(D_{11})^2 + (D_{22})^2 + (C_1)^2 + (C_2)^2}$$

$\Rightarrow$ MMPDEs are derived from variational principles as a minimiser of mapping functional

$$\mathcal{I}[\bar{\mathbf{x}}] = \frac{1}{2}\int_{\mathcal{D}_p} \sum_{k=1}^{2} (\nabla \bar{x}^k)^T\, M^{-1}\,\nabla \bar{x}^k\, d\mathbf{x}$$

ECMWF

One-dimensional stationary view on the MMPDE:

$$\mathcal{I}[\overline{x}] = \frac{1}{2} \int_{\mathcal{D}_p} \frac{1}{m} \left(\frac{\partial \overline{x}}{\partial x} \right)^2 dx$$

with Euler-Lagrange equation

$$\frac{\partial}{\partial \overline{x}} \left(m(x) \frac{\partial x}{\partial \overline{x}} \right) = 0 \; + \text{BCs}$$

$m(x) : \mathbf{S}_p \to \mathbb{R}^+$ is monitor function to control local mesh spacing

Moving mesh PDEs

- Example:

  $x(0) = 0, \;\; x(1) = 1$
  $\overline{x}(0) = 0, \;\; \overline{x}(1) = 1$

  $m(x) = 1$

$$\frac{\partial}{\partial \overline{x}} \left(m(x) \, \frac{\partial x}{\partial \overline{x}} \right) = 0$$

$$\Rightarrow \quad x = x(\overline{x})$$

Number of grid increments: $N = 20$

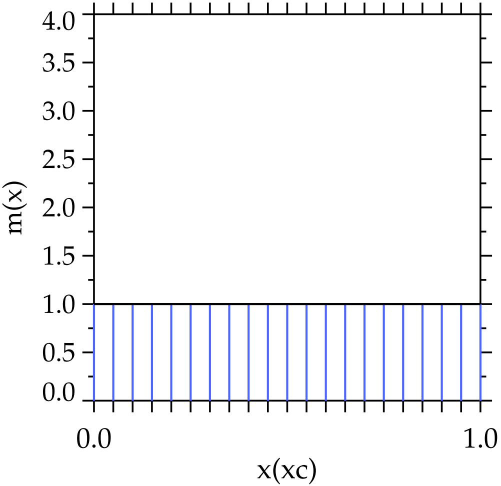

- Example:

  $x(0) = 0, \ \ x(1) = 1$
  $\overline{x}(0) = 0, \ \ \overline{x}(1) = 1$

  $m(x) = \exp\left(x \ \ln 2\right)$

$$\frac{\partial}{\partial \overline{x}} \left(m(x) \, \frac{\partial x}{\partial \overline{x}} \right) = 0$$

$$\Rightarrow \quad x = x(\overline{x})$$

Number of grid increments: $N = 20$

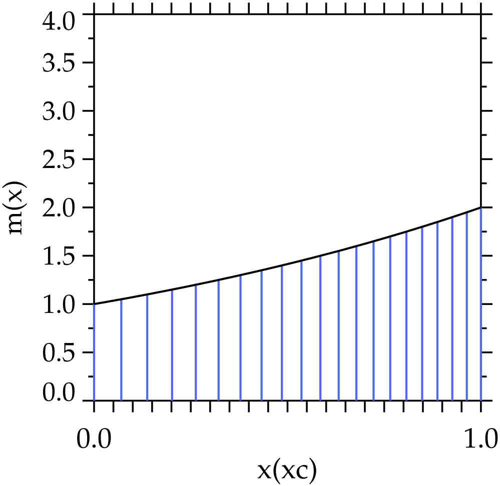

- Example:

$$x(0) = 0, \quad x(1) = 1$$
$$\overline{x}(0) = 0, \quad \overline{x}(1) = 1$$

$$m(x) = \exp\left(x \ln 4\right)$$

$$\frac{\partial}{\partial \overline{x}} \left(m(x) \, \frac{\partial x}{\partial \overline{x}} \right) = 0$$

$$\Rightarrow \quad x = x(\overline{x})$$

Number of grid increments: $N = 20$

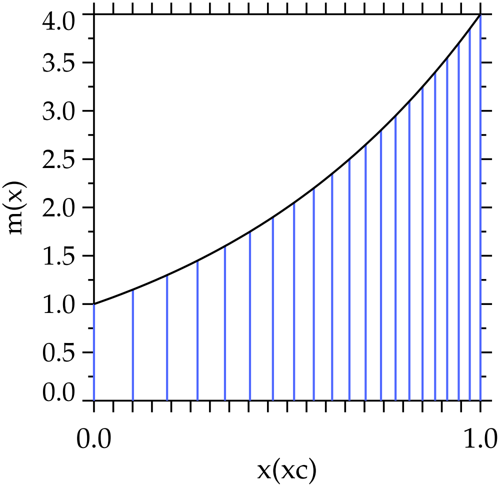

Moving mesh PDEs

→ Monitor function M (2×2 matrix in 2D):

$$M = I\, q$$

with scalar weighting function

$$q(t, \mathbf{x}_h) = 1 + \frac{\beta}{1-\beta}\, \frac{\Phi}{\langle \Phi \rangle_h}\ , \qquad\qquad I \text{ is identity matrix}$$

→ Φ is mesh refinement indicator; $\langle \Phi \rangle_h$ denotes its horizontal average

→ $0 \le \beta < 1$ controls strength of adaptation

→ q is filtered to obtain good quality mesh

Moving mesh PDEs

→ Monitor function M (2×2 matrix in 2D):

$$M = I\, q$$

with scalar weighting function

$$q(t, \mathbf{x}_h) = 1 + \frac{\beta}{1-\beta}\,\frac{\Phi}{\langle\Phi\rangle_h}\,, \qquad I \text{ is identity matrix}$$

→ Φ is mesh refinement indicator; $\langle\Phi\rangle_h$ denotes its horizontal average

→ $0 \le \beta < 1$ controls strength of adaptation

→ q is filtered to obtain good quality mesh

→ boundary conditions of 2D MMPDEs are either of Dirichlet-type for $\mathbf{x}_h$ found by means of 1D MMPDEs

$$p(s,\mu)\,\frac{\partial s}{\partial \bar{t}} = \mu\,\frac{\partial^2 s}{\partial \bar{s}^2} + \frac{\partial \mu}{\partial \bar{s}}\,\frac{\partial s}{\partial \bar{s}}$$

along boundary segments or are assumed periodic, depending on BC of the model

Adaptive moving mesh solver

- Mesh adaptation module
  - · Compute monitor matrix M^n using Ψ^n
  - · Advance boundary mesh $\mathbf{x}_b^n \rightarrow \mathbf{x}_b^{n+1}$ using 1D MMPDEs (3.9)
  - · Advance mesh $\mathbf{x}^n \rightarrow \mathbf{x}^{n+1}$ using 2D MMPDEs (3.6)

- Compute metric coefficients from $\mathbf{x}^{n+1}$

- Predict advective flux $(\rho^* \overline{\mathbf{v}}^*)^{n+1/2}$

- Advance all physical fields $\Psi^n \rightarrow \Psi^{n+1}$

- Time step adaptation $\delta \overline{t}^n \rightarrow \delta \overline{t}^{n+1}$

· In framework of two-time-level flow solver EULAG (Prusa et al. CF 2008, Kühnlein et al. JCP 2012)

Combining the soundproof and compressible PDE solver (Smolarkiewicz et al. JCP 2014) with adaptive moving meshes:

$$(\overline{x}, \overline{z}) = (E(t,x,z), D(t,x,z)) : \quad \mathcal{D}_p \to \mathcal{D}_t$$

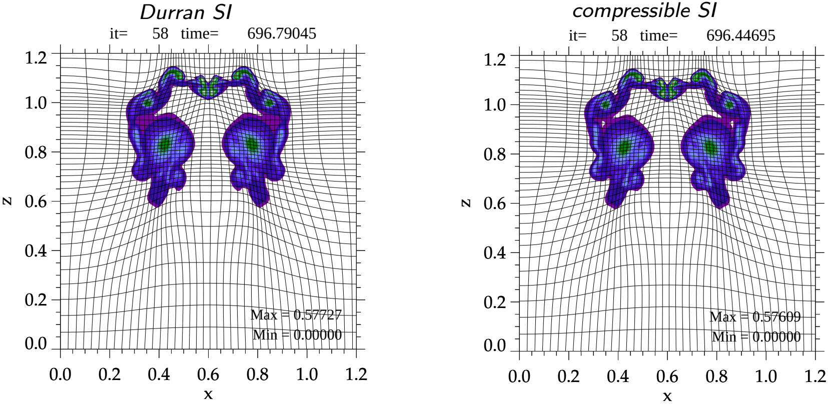

→ mesh refinement indicator: $\Phi = ||\nabla\theta||$

- $\rightarrow$ zonally-periodic channel 10000 km $\times$ 8000 km $\times$ 18 km
- $\rightarrow$ baroclinically unstable jet flow (Bush and Peltier, JAS 1994)
- $\rightarrow$ perturb initial state by local θ-anomaly at tropopause
- $\rightarrow$ integrate for 12 days

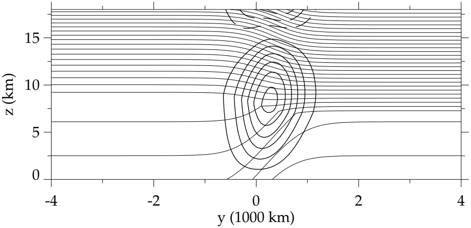

- $\rightarrow$ Coordinate mapping:

$$(\bar{x}, \bar{y}, \bar{z}) = (E(t,x,y), D(t,x,y), C(t,x,y,z)) : \quad \mathcal{D}_p \rightarrow \mathcal{D}_t$$

Baroclinic wave life cycle experiments with adaptive moving meshes

- → zonally-periodic channel 10000 km × 8000 km × 18 km
- → baroclinically unstable jet flow (Bush and Peltier, JAS 1994)
- → perturb initial state by local θ-anomaly at tropopause
- → integrate for 12 days

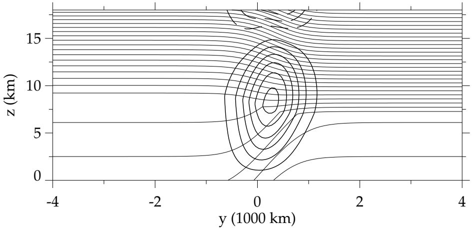

- → Coordinate mapping:

$$(\overline{x}, \overline{y}, \overline{z}) = (E(t,x,y), D(t,x,y), C(t,x,y,z)) : \quad \mathcal{D}_p \to \mathcal{D}_t$$

Baroclinic wave life cycle experiments with adaptive moving meshes

(Kühnlein et al. JCP 2012)

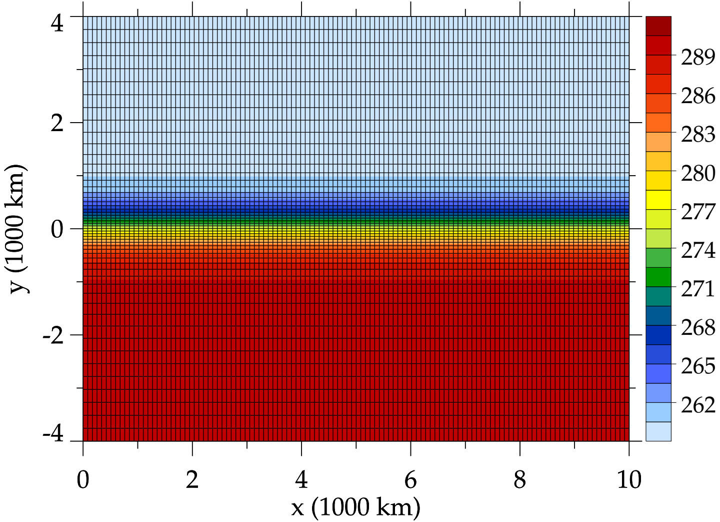

→ mesh refinement indicator: $\Phi = ||\nabla_h \theta(z = 600\,\mathrm{m})||$

Baroclinic wave life cycle experiments with adaptive moving meshes

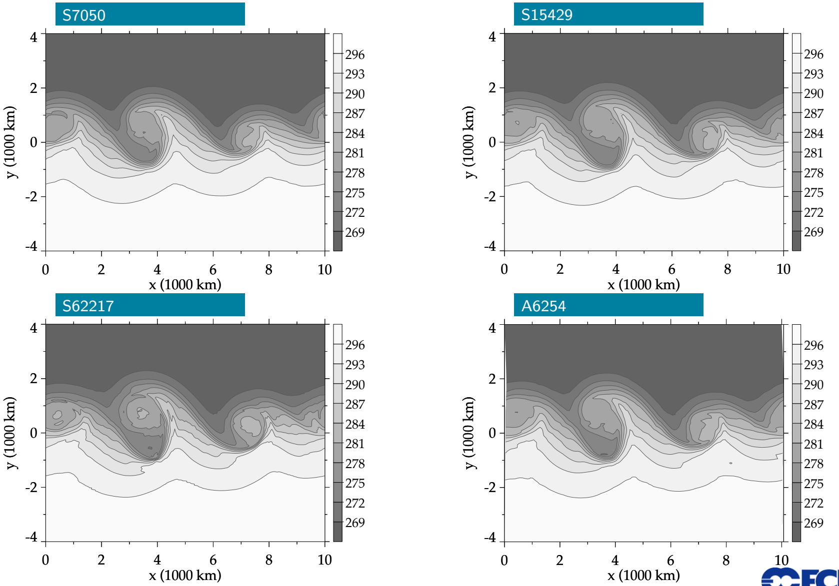

temperature field at $z = 2$ km and $t = 234$ h

Domain-averaged kinetic energetics with integration time

total kinetic energy $\langle \mathrm{KE} \rangle$

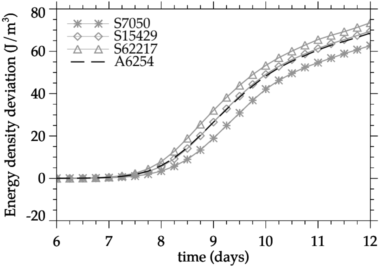

eddy kinetic energy $\langle \mathrm{EKE} \rangle$

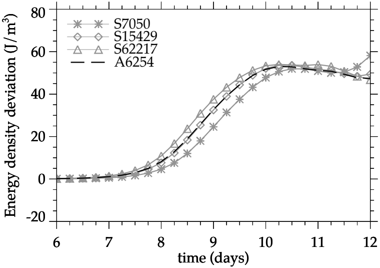

zonal kinetic energy $\langle \mathrm{ZKE} \rangle$

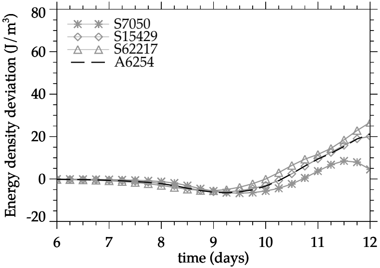

Simulation	Refinement indicator $\Phi(t, x, y)$	$\mathcal{E}_{\langle \mathrm{KE} \rangle}$	$\mathcal{E}_{\langle \mathrm{ZKE} \rangle}$	$\mathcal{E}_{\langle \mathrm{EKE} \rangle}$
S7050	-	6.43	4.99	4.84
S15429	-	2.58	1.66	1.90
A6254a	$\frac{1}{H} \int_0^H \lVert \nabla_h \theta \rVert \, dz$	2.82	1.67	1.80
A6254b	$\lVert \nabla_h \theta (z = 600 \text{ m}) \rVert$	3.75	2.64	2.28
A6254c	$\lVert \nabla_h \theta (z = 3000 \text{ m}) \rVert$	2.91	1.57	1.92
A6254d	$\lVert \nabla_h \theta (z = 5100 \text{ m}) \rVert$	2.98	2.43	1.98
A6254e	$\frac{1}{H} \int_0^H \lVert \nabla \times \mathbf{v} \rVert \, dz$	2.90	2.10	1.83
A6254f	$\frac{1}{H} \int_0^H \lvert PV \rvert \, dz$	3.81	2.31	2.45
A6254g	$\lvert PV(z = 5100 \text{ m}) \rvert$	4.65	2.48	2.97
A6254h	$\lvert PV(z = 9000 \text{ m}) \rvert$	4.22	2.62	2.64
A6254i	$\frac{1}{H} \int_0^H \lVert \nabla_h PV \rVert \, dz$	3.82	2.36	2.65
A6254j	$\frac{1}{H} \int_0^H \lvert PV \rvert \, dz \, , \, \frac{1}{H} \int_0^H \lVert \nabla_h PV \rVert \, dz$	3.84	2.27	2.52
A6254k	$\frac{1}{H} \int_0^H \lvert EPV \rvert \, dz$	10.77	5.43	8.57
A6254l	$\lvert EPV(z = 5100 \text{ m}) \rvert$	9.50	4.60	7.56

$$\mathcal{E}_{\vartheta} = \left(\frac{1}{N_o} \sum_{i=1}^{N_o} \left(\vartheta_i - \vartheta_i^R \right)^2 \right)^{1/2} \qquad \forall \quad \vartheta = \langle \mathrm{KE} \rangle \, , \langle \mathrm{ZKE} \rangle \, , \langle \mathrm{EKE} \rangle$$

$\rightarrow$ ϑ^R is high-resolution reference simulation S62217 with static uniform mesh

$\rightarrow$ $N_o = 48$ is number of 6-hourly model outputs over integration period of 12 days

Multiscale performance

→ Representation of internal gravity waves occurring in response to imbalances in the evolving baroclinic wave flow:

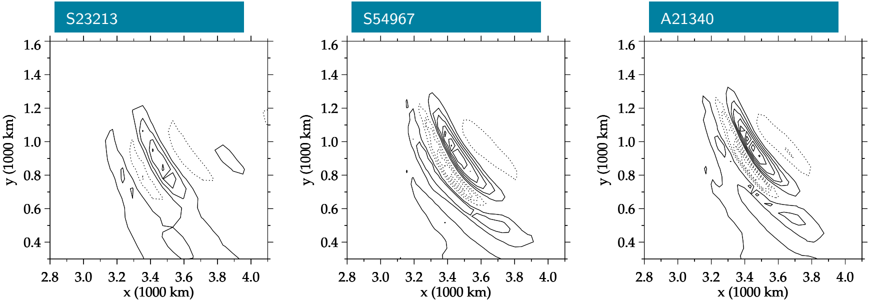

vertical velocity field at $z = 12$ km and $t = 246$ h

Adaptive moving meshes on the sphere

→ Mesh generation using optimal transport (Weller et al. JCP 2016):

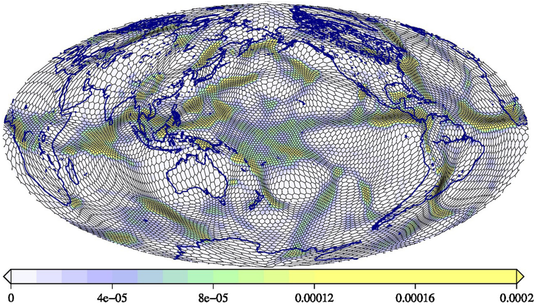

Adaptive moving meshes:

+ efficient way of employing mesh adaptivity
+ keeps grid/data structure
- less flexible than h- or hr-adaptive techniques

→ Mesh refinement criteria ?

→ Subgrid-scale parameterisations ?

→ ...

- Behrens, "Adaptive atmospheric modeling", Springer 2006
- Weller et al. BAMS 2010